Title

Tailoring Spin Textures in Complex Oxide Micromagnets.

Journal

ACS nano, 10(9)

ISSN

1936-0851

Authors

Lee, Michael S

Wynn, Thomas A

Folven, Erik

et al.

Publication Date

2016-09-14

DOI

10.1021/acsnano.6b03770

Peer reviewed

ACSNANO
www.acsnano.org
ARTICLE

Tailoring Spin Textures in Complex Oxide Micromagnets

Michael S. Lee,[†,⊥] Thomas A. Wynn,[†,⊥] Erik Folven,[‡] Rajesh V. Chopdekar,[†] Andreas Scholl,[§] Anthony T. Young,[§] Scott T. Retterer,[∥] Jostein K. Grepstad,[‡] and Yayoi Takamura*[,†]

[†]Department of Materials Science and Engineering, University of California—Davis, Davis, California 95616, United States
[‡]Department of Electronics and Telecommunications, Norwegian University of Science and Technology, NO-7491 Trondheim, Norway
[§]Advanced Light Source, Lawrence Berkeley National Laboratory, Berkeley, California 94703, United States
[∥]Center for Nanophase Materials Sciences, Oak Ridge National Laboratory, Oak Ridge, Tennessee 37831, United States

Supporting Information

ABSTRACT: **Engineered topological spin textures with submicron dimensions in magnetic materials have emerged in recent years as the building blocks for various spin-based memory devices. Examples of these magnetic configurations include magnetic skyrmions, vortices, and domain walls. Here, we show the ability to control and characterize the evolution of spin textures in complex oxide micromagnets as a function of temperature through the delicate balance of fundamental materials parameters, micromagnet geometries, and epitaxial strain. These results demonstrate that in order to fully describe the observed spin textures, it is necessary to account for the spatial variation of the magnetic parameters within the micromagnet. This study provides the framework to accurately characterize such structures, leading to efficient design of spin-based memory devices based on complex oxide thin films.**

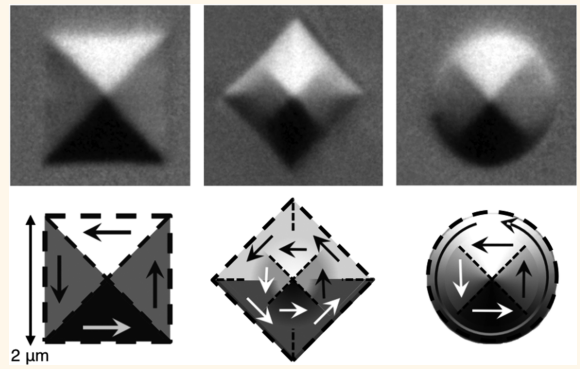

KEYWORDS: *complex oxides, micromagnetics, magnetic anisotropy, X-ray photoemission electron microscopy*

Spin textures consist of spatially varying spin arrangements that form within patterned magnetic materials with nano-/microscale dimensions and are considered to have substantial promise as the basis for spin-based memory devices.[1−7] In particular, magnetic skyrmions have received significant interest for future spintronic devices as they exhibit phenomena including topological electric and spin Hall effects[8−10] and microwave magnetoelectric effects[11] and they require much lower critical current densities for propagation by spin-transfer torque than other forms of spin textures such as domain walls.[6,12,13] In an effort to find materials and feature geometries more amenable to the incorporation of magnetic skyrmions into functional devices, recent work has focused on specially designed metal heterostructures with spatially divergent spin−orbit torque[14] and embedding a magnetic vortex in a perpendicular spin environment.[15] However, a thorough understanding of the spatial variation of fundamental magnetic parameters in nano/microstructures remains largely unexplored despite the fact that in many classes of materials, but especially complex oxides, functional properties are sensitively correlated to lattice strains.[16] This issue will only grow in significance as spin-based devices with increasingly complex spin textures become more commonplace, such that the integration of the magnetic layers with various device components including the substrate, contacts, and isolations regions must be considered. For example, synchrotron X-ray microdiffraction experiments have shown lattice nonuniformities within the strained silicon gate of a metal-oxide semiconductor field-effect-transistor due to the different types of interfaces and surfaces, which ultimately modify the local electron mobility.[17] Similar work utilizing coherent X-ray diffraction on individual $LiNi_{0.5}Mn_{1.5}O_{4-\delta}$ cathode nanoparticles demonstrated that inhomogeneous strain influences electrochemical performance and is dependent on environment, size, and geometry.[18]

In order to effectively probe the modification in magnetic behavior when a continuous epitaxial thin film is patterned into micromagnets of varying size and shape, a material with observable properties sensitive to slight perturbations caused by

Received: June 7, 2016
Accepted: September 11, 2016
Published: September 12, 2016

DOI: 10.1021/acsnano.6b03770
ACS Nano 2016, 10, 8545−8551

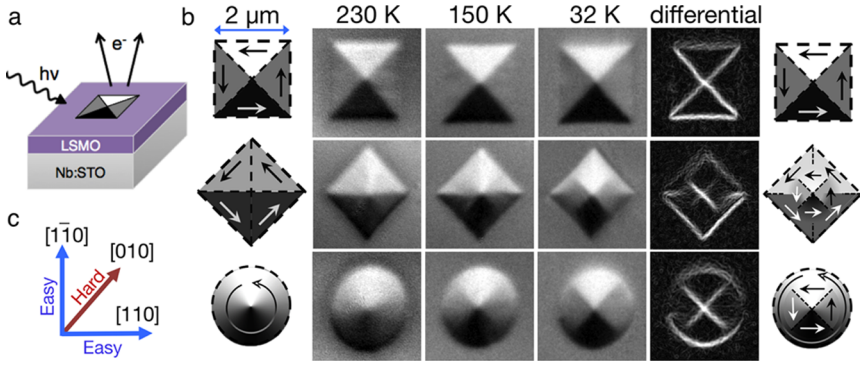

Figure 1. Magnetic domain images of patterned micromagnets. (a) Experimental setup of the PEEM3 microscope. (b) Temperature-dependent XMCD-PEEM images of the magnetic domains in square, diamond, and circular micromagnets. Contrast is normalized in all images/temperatures to better observe domain structure evolution. Differential images highlight domain boundaries of the domain images acquired at 32 K. Schematics indicate the direction of magnetic moments within the domains. (c) Orientation of the magnetic easy and hard axes of the LSMO thin film.

the fabrication process must be studied. Complex oxides such as $La_{0.7}Sr_{0.3}MnO_3$ (LSMO) satisfy this requirement as they offer a wide range of highly tunable functional properties and display strong correlations between the spin, charge, orbital, and lattice degrees of freedom. These factors may also provide a versatile route to control spin textures and magnetic behavior in nano/micro-patterned structures. This is extremely relevant when designing vortex core dynamics for application in future data storage technologies, as the stability and control of such systems are heavily influenced by the magnetic energy landscape.[19] LSMO is a soft ferromagnetic metal, which displays coincident ferromagnetic/paramagnetic and metal/insulator transitions, a large peak in magnetoresistance (i.e., colossal magnetoresistance, CMR) at its Curie temperature (T_C), and a high-degree of spin-polarization, which is essential for efficient spin-transfer torque applications.[20,21] In epitaxial thin films, magnetocrystalline anisotropy directly impacts the formation and configuration of spin textures and can be the dominant driving force in stabilizing the magnetic state of spin-based memory devices.[2]

Enabled by a unique patterning technique designed for complex oxides[22,23] and high-resolution imaging of spin configurations using X-ray photoemission electron microscopy (X-PEEM), we show the evolution of spin textures in complex oxide micromagnets and devise a framework in which the lateral variation of fundamental materials' parameters, including saturation magnetization and magnetocrystalline anisotropy constants, can be determined as a function of temperature with approximately 0.1 μm spatial resolution.

RESULTS AND DISCUSSION

Arrays of micromagnets were defined in a 100 unit cell thick epitaxial film of LSMO using a patterning technique based on the local modification of the structural and magnetic order by Ar^+ ion implantation.[22,23] Three different geometries were patterned: squares with 2 μm long edges oriented along the in-plane ⟨110⟩ substrate directions, squares of the same dimensions with edges along the in-plane ⟨100⟩ substrate directions (referred to as diamonds), and circles with a diameter of 2 μm. Each shape provides a unique perspective on the balance of relevant magnetic energies. For LSMO films grown under tensile strain on (001)-oriented $SrTiO_3$ (STO) substrates, the magnetic easy axes have been shown to lie along the in-plane ⟨110⟩ directions.[24] Thus, in the square micromagnets, both shape and magnetocrystalline anisotropy promote the same Landau flux closure structure with moments aligned parallel to the edges, whereas those energy terms are at odds with one another in the diamond micromagnets. Similarly, circular micromagnets typically display a vortex structure characterized by a continuous rotation of moments tangential to the edge at the expense of magnetocrystalline anisotropy energy. The 2 μm wide micromagnets studied here lie in the size regime where new domain walls will not be injected to form more complicated multidomain states but they are still large enough to observe subtle details in domain structure due to magnetocrystalline anisotropy.[25,26] For micromagnets with smaller dimensions (e.g., 500 nm wide) patterned in LSMO as well as metallic nano- and micromagnets, domain patterns dictated by shape anisotropy were observed irrespective of the shape (i.e., square, diamond, or circle).[19,27] Theoretically, many types of ferromagnetic materials with a similar balance of saturation magnetization, M_S, and magnetocrystalline anisotropy, K_1, ($K_1/M_S \sim -0.01$ T for LSMO) should produce comparable magnetic domain structures including metals, other oxides, and Heusler alloys (e.g., Fe, Fe_3O_4, and Co_2FeAl); however, it is necessary that they are epitaxial or single crystalline and are characterized by a technique sensitive to the in-plane magnetization (e.g., X-PEEM or spin-polarized low energy electron microscopy).

The magnetic domain patterns (Figure 1) were imaged with high spatial resolution (~40 nm) and as a function of temperature from T_C to 32 K using X-PEEM at the PEEM3 endstation on beamline 11.0.1 of the Advanced Light Source. The magnetic contrast in X-PEEM arises due to X-ray magnetic circular dichroism (XMCD) at the Mn $L_{3,2}$ absorption edges of LSMO, and it scales with the dot product between the local magnetization and the helicity of the X-rays beam (horizontal in Figure 1, oriented along the [110] easy axis).[28] Thus, domains with the brightest/darkest/intermediate contrast correspond to regions with the magnetic moments aligned antiparallel/parallel/perpendicular to the helicity of the X-rays, respectively. The schematics in Figure 1 highlight the magnetic domain orientation based on the XMCD contrast.

As shown in Figure 1b (left column), at 230 K, the micromagnets display domain patterns dominated by shape anisotropy (i.e., Landau or vortex domain states where the magnetization follows the edges of the structures). For the diamond micromagnets, the two top (bottom) domains are

DOI: 10.1021/acsnano.6b03770
ACS Nano 2016, 10, 8545−8551

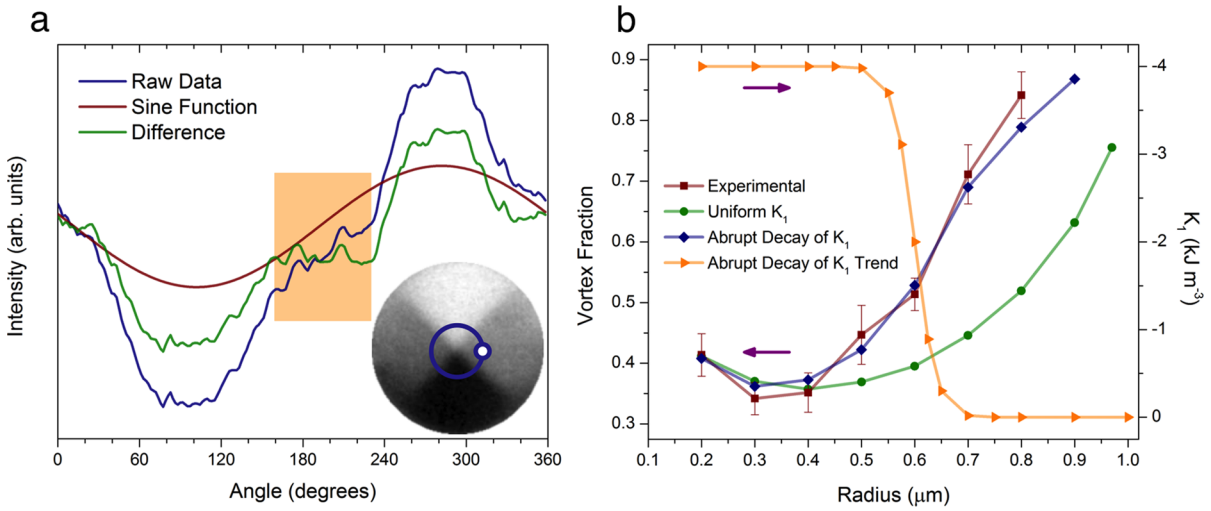

Figure 2. Determination of magnetocrystalline anisotropy constants from hybrid spin textures. (a) Intensity vs angle extracted from a circular profile of radius = 0.3 μm in a circular micromagnet at 32 K (see inset). The highlighted region denotes the angular range where deviation from the step function is most obvious in the raw data. Subtraction of a sine function (red line) from the raw data (blue line) results in an approximate step function (green line). The white dot in the inset denotes the start position for the circular profiles taken in a clockwise direction. (b) Vortex fraction f_v vs radius for X-PEEM data (red line) and simulations using a uniform K_1 value (green line) or an abrupt decay of K_1 profile (blue line). The abrupt decay of K_1 profile consists of a sigmoid function with an abrupt change at a radius = 0.6 μm (orange line).

indistinguishable from one another since they have the same component of magnetization in the direction of the helicity of the X-rays. A vertical stripe of higher/lower intensity through the center of the diamond arises due to the domain wall where the moments are aligned antiparallel/parallel to the X-ray beam, whereas the moments in the two adjacent domains form a 45° angle. This domain structure agrees with previous results from 500 nm wide structures in LSMO[22] and metal alloys with a low magnetocrystalline anisotropy.[19,27] As the temperature is reduced to 32 K, no change is observed in the domain patterns for the square micromagnets.

For both the diamond and circular micromagnets, the domain patterns change substantially: a clear Landau pattern in the center of the structure can be seen with the magnet moments aligned along the ⟨110⟩ easy axes. The magnetization in the perimeter region (~0.15 μm wide) remains oriented by shape anisotropy. The schematics on the right-hand side of Figure 1b show that for the diamond micromagnets, this domain pattern consists of two concentric Landau patterns rotated by 45° relative to one another. Similarly for the circular micromagnets, the domain pattern consists of a ⟨110⟩-oriented Landau pattern surrounded by a thin region with a vortex structure. The derivatives of the domain images (differential images in Figure 1b) highlight the locations of the domain walls associated with the Landau patterns. For these micromagnets, the central Landau pattern gives rise to domain walls forming a central "X". For the diamond micromagnets, two horizontal spurs emanate from the right/left corners resulting from the outer Landau pattern. A gradual development of the inner Landau pattern can be seen at intermediate temperatures. The existence of these unique spin textures in the form of double concentric flux closure patterns results from the delicate, spatially dependent balance between shape and magnetocrystalline anisotropy energies, and it demonstrates our control of spin textures in complex oxides structures.

To understand the formation of the double concentric flux closure domains in the diamond and circular micromagnets, micromagnetic simulations were performed using MuMax3,[29] which takes the sample geometry, as well as values for M_S, K_1, and exchange stiffness (A_{Ex}) as inputs to calculate the lowest energy state of a magnetic feature using the Landau–Lifshitz–Gilbert equation.[29] The temperature dependence of M_S was determined for an unpatterned LSMO film grown with the same deposition conditions using a superconducting quantum interference device magnetometer. The intensity difference between the bright and dark domains of the X-PEEM images for the square micromagnets was used to determine the local saturation magnetization of the patterned structures. The experimental domain contrast was found to be homogeneous throughout each domain at each measurement temperature (see Supporting Information Figure S1). This analysis predicts a $T_C \sim 270$ K, comparable to the as-deposited film, confirming that bulk magnetic behavior is retained within the patterned structures. The relationship between M_S and A_{Ex} can be described as

$$A_{Ex} = \frac{D_{sp} M_s}{2g\mu_B} \quad (1)$$

where g is the Landé factor, μ_B is the Bohr magneton, and D_{sp} is the spin wave stiffness constant. Temperature-dependent values of D_{sp} for LSMO films on STO substrates, as determined by Golosovsky et al. using magnetic-field-dependent microwave absorption, were used to calculate A_{Ex}.[30] The remaining unknown is the magnetocrystalline anisotropy constant, K_1. Previously, Steenbeck et al.[31] examined the temperature dependence of K_1 in 26 nm thick LSMO films grown on STO substrates by torque magnetometry and found a monotonic increase with decreasing temperature (Figure 3). The simulation cell volume of 5 × 5 × 40 nm^3 assumes magnetic parameters are constant throughout the depth of the film.

The X-PEEM images for the circular micromagnets were quantitatively compared with micromagnetic simulations as a function of temperature using a metric termed the *vortex*

DOI: 10.1021/acsnano.6b03770
ACS Nano 2016, 10, 8545–8551

fraction (f_v). Assuming a pure vortex structure, the contrast around a circular profile (such as along the blue circle in the inset to Figure 2a) should be sinusoidal as a function of angle. For a pure Landau structure (as in the square micromagnets), the contrast should remain constant within a single domain, and the circular intensity profile will result in a step function with sharp steps every 90° (see Supporting Information Figure S2). The experimental profile obtained from a circle with radius = 0.3 μm (blue circle in the inset to Figure 2a) has abrupt changes in contrast at the domain walls but also displays an intensity that is not constant within each of the four domains (blue curve in Figure 2a). The deviation from the step function of the Landau structure is particularly apparent within the gray domains (highlighted regions in Figure 2a). This behavior indicates the local moments are not perfectly parallel within each magnetic domain but rather are characterized by some degree of rotation akin to a vortex structure. A superposition of a step function (Landau structure) and a sine function (vortex structure) more accurately describes the spin texture of the micromagnets. By subtracting a sine function from the experimental data, the difference (green curve in Figure 2a) has the expected step profile of a Landau pattern. The vortex fraction, f_v, quantifies the relative proportions of Landau and vortex structures as

$$f_v = \frac{A_{sine}}{A_{sine} + A_{step}} \quad (2)$$

where A_{sine} is the amplitude of the subtracted sine function (vortex component) and A_{step} is the amplitude of the remaining step function (Landau component). Figure S4 illustrates fit quality for the raw data in Figure 2a. In addition to the sine and step functions, linear regions are spliced into the fit accounting for rapid changes in contrast due to domain walls but do not influence the amplitude used to calculate f_v. The vortex fraction was extracted as a function of both the radius within the circular micromagnet (Figure 2b) and as a function of temperature. Shape anisotropy dominates at the perimeter of the circular micromagnet, so that f_v approaches unity at larger radii. The vortex fraction decreases as the radius decreases as the influence of magnetocrystalline anisotropy overcomes that of shape anisotropy and the Landau structure emerges. The magnitude of this decrease is enhanced at lower temperatures. Finally, near the center of the micromagnet, f_v increases again due to the formation of the vortex core with an out-of-plane component, convoluted with the limitations in the spatial resolution of the PEEM3 microscope.

Micromagnetic simulations also yield the superposition of the Landau and vortex components in the spin texture of the micromagnets, thus allowing f_v to be used to accurately select the simulation parameters that best correspond with X-PEEM images at a given temperature. A series of simulations with a range of K_1 values and with varying K_1 profiles was carried out for each pair of M_S and A_{Ex} values as a function of radius for the temperature range from 32−230 K. The simple assumption of a uniform K_1 profile throughout the micromagnet (green line in Figure 2b) only matches the observed f_v values in the central region (0.2 μm < radius < 0.4 μm). At larger radius, the simulations underestimate f_v, suggesting that K_1 decreases toward the perimeter of the micromagnet (see Supporting Information Figure S3). Simulations with a gradually decreasing K_1 profile also underestimate f_v, at large radius. Of all tested decay models, the full f_v radial dependence (blue line in Figure 2b) was best represented using a sigmoid function with an abrupt change in K_1 at a radius = 0.6 μm. The X-PEEM and MuMax[3] images do not show a corresponding abrupt change in the domain patterns at this radius due to the fact that the exchange energy works to smooth out any sharp changes in local magnetization. These result highlight the fact that spatial variation in all fundamental magnetic parameters must be accounted for to accurately model the magnetic domains in patterned media, as K_1 values at the inner region of the micromagnet directly affect the domain patterns of the outer region, and vice versa. The different radial dependencies of M_S and K_1 are surprising, however, it has been reported that substrate-induced strain modifies the T_C[32] and low temperature K_1 values[33] of an epitaxial LSMO film. In addition, Thiele et al. studied the relationship between strain-induced changes in T_C and magnetization and discovered that though the T_C may change with strain, changes in saturation field and M_S at low temperatures are negligible.[34] Therefore, it is possible that at low temperatures, K_1 is reduced by strain from the surrounding matrix, whereas M_S remains unchanged.

The temperature dependence of K_1 was determined assuming both a uniform and abruptly varying K_1 profiles as shown in Figure 3. For the uniform K_1 profile, the K_1 values

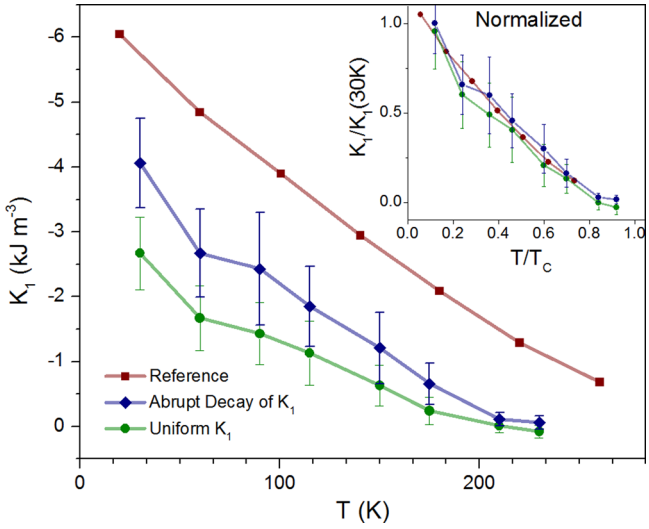

Figure 3. Temperature-dependent magnetocrystalline anisotropy. Magnetocrystalline anisotropy constants as a function of temperature using a uniform (green line) and abruptly varying K_1 profile (see text for details, blue line). For comparison, reference data for a thin film is also included (red line).[31] The inset shows data normalized to T/T_C and K_1/K_1(30 K), showing excellent agreement.

were determined as the average value in the central region (0.2 μm < radius < 0.4 μm), while for the abruptly varying K_1 profile, the maximum value of the sigmoidal function was used. Both calculated values display a similar trend with temperature as those presented by Steenbeck et al.[31] Because the LSMO thin films studied by Steenbeck et al. had higher M_S and T_C values, the data is plotted on normalized axes in the inset to Figure 3, which confirms that all three curves possess analogous temperature dependence. In order to illustrate that the temperature-dependent K_1 values extracted from the X-PEEM images are the essential parameters for the determination of the experimentally observed spin textures, micromagnetic simulations of the square, diamond, and circular micromagnets are

DOI: 10.1021/acsnano.6b03770
ACS Nano 2016, 10, 8545−8551

shown in Figure 4 for the three temperatures from Figure 1. Excellent agreement exists between the two sets of images.

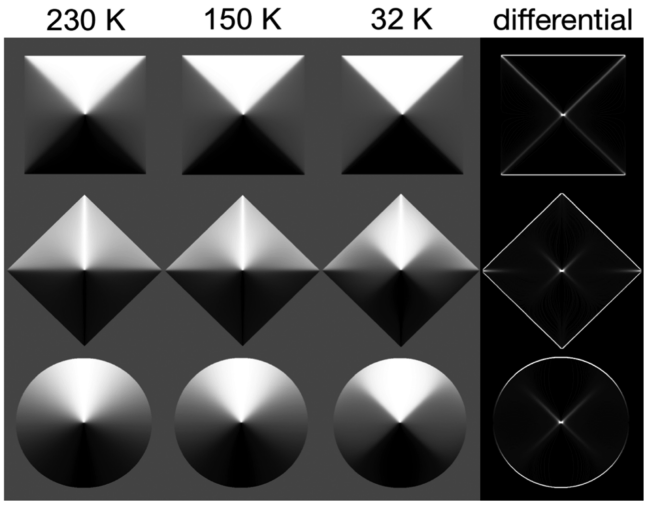

Figure 4. Simulated magnetic domain images. Simulated magnetic domain images at the same temperatures from Figure 1 and associated differential images (T = 32 K) using the calculated values of K_1.

The results shown in Figure 3 suggest that the inner region of the micromagnets (radius < 0.6 μm) has bulk-like magnetic properties when plotted on normalized scales to account for the reduced T_C and M_S of the sample due to the specific growth conditions used, whereas additional phenomena must be considered at the perimeter. The lateral extent of this low K_1 region surpasses the distance over which the vortex structure emerges near the edge of the circular micromagnets at 32 K in the X-PEEM images (approximately 0.15 μm). Furthermore, contrast, and thus magnetization, within each domain in the square micromagnets is radially uniform, showing no correlation to the variance of K_1 (see Supporting Information Figure S1). The patterning processed used in this work results in magnetic islands embedded within a nonmagnetic matrix that has undergone a structure modification due to the Ar^+ ion bombardment.[22] Damage from ion implantation straggle as calculated with Stopping and Range of Ions in Matter reveals that the magnetization should not be affected beyond 40 nm from the edge of the hard mask under the conditions used.[35] The expansion and disruption of the lattice structure of the surrounding matrix may lead to local changes in the epitaxial strain state at the island/matrix interface, both in the in-plane and out-of-plane directions, which competes with the in-plane tensile strain imposed from the underlying STO substrate. X-ray microdiffraction studies of ferroelectric domain walls in $BaTiO_3$ show that triaxial residual strain of this magnitude can propagate several microns in complex oxides[36] and that length scale is consistent with the observed deviation in K_1 in the microstructures presented here. We note that an analogous explanation was postulated for the edge-imposed alignment of the antiferromagnetic spin axis in patterned structures in $LaFeO_3$ thin films and $LaFeO_3$/LSMO bilayers.[37−39]

CONCLUSIONS

In conclusion, unique spin textures in the form of double concentric flux closure patterns have been observed and characterized in micromagnets patterned into an epitaxial LSMO thin film. These spin textures originate from the delicate balance between shape and magnetocrystalline anisotropy energies and demonstrate the tunability of magnetic parameters in complex oxides through methods such as nanostructuring and local strain engineering. The spatial variation of the fundamental magnetic parameters is essential to fully describe observed spin textures, and we have demonstrated a framework to acquire key magnetic parameters, namely magnetocrystalline anisotropy constants, in micromagnets with sub-0.1 μm spatial resolution. These results are generally applicable to epitaxial films of ferromagnetic materials with a similar balance between saturation magnetization and magnetocrystalline anisotropy and they enhance our capability to design and characterize functional properties of future spin texture-based devices.

METHODS/EXPERIMENTAL

A 100 unit-cell-thick LSMO thin film was grown epitaxially by pulsed laser deposition on a (001)-oriented Nb-doped (0.05 wt % Nb) STO substrate. During growth, the substrate temperature was held at 680 °C, and the oxygen pressure was 2.0×10^{-1} mbar. A KrF excimer laser was operated at fluence of 2.0 J/cm^2 and 1 Hz repetition rate. The growth was monitored with *in situ* reflection high-energy electron diffraction, and unit-cell intensity oscillations of the specular reflection were observed throughout the growth. Structural analysis was performed with X-ray diffraction and X-ray reflectivity using a four-circle Bruker D8 Discover to verify film crystallinity, epitaxial nature, and thickness. Microstructures (~100 of each geometry) were defined using a patterning technique based on local modification of the structural and magnetic order by Ar^+ ion implantation through a Cr hard mask.[22,23] Scanning electron microscopy was performed at room temperature to verify the shape and size of the nanostructures. X-PEEM images were acquired using right and left circularly polarized (RCP and LCP, respectively) X-rays at a photon energy corresponding to the maximum XMCD signal at the Mn L_3 edge of the film. The domain images were obtained using an asymmetry equation, $I = (I_{RCP} - I_{LCP})/(I_{RCP} + I_{LCP})$, which removes contributions from topography and work function differences from the individual images. The X-ray beam was incident along the [110] direction at 30° from the sample surface, and the PEEM3 chamber was shielded from external magnetic fields so that all images correspond to the demagnetized state. K_1 error bars are derived from variations in the experimental f_v value obtained from four individual micromagnets taken with high resolution images. X-PEEM image contrast is only sensitive to the in-plane magnetization component parallel to the incident beam, but MuMax^3 simulations output a complete vector field. The images generated by MuMax^3 shown and studied here are obtained by using only the x component of the vector field, which is analogous to the X-PEEM measurements. A full listing of simulation parameters can be found in Table SI of the Supporting Information.

ASSOCIATED CONTENT

Supporting Information

The Supporting Information is available free of charge on the ACS Publications website at DOI: 10.1021/acsnano.6b03770.

Supporting Information describing radial dependence of magnetization within an individual micromagnet (Figure S1), a full spectrum of radial profiles (Figure S2), further detail of magnetocrystalline anisotropy constants (Figure

DOI: 10.1021/acsnano.6b03770
ACS Nano 2016, 10, 8545−8551

S3), an example fit of circular profile data (Figure S4), and a complete list of the simulation parameters used (Table S1) are presented. (PDF)

AUTHOR INFORMATION

Corresponding Author

*E-mail: ytakamura@ucdavis.edu. Phone: 530-754-7124. Fax: 530-752-1031. Address: Department of Materials Science and Engineering University of California—Davis, One Shields Avenue, Davis, CA 95616, United States.

Author Contributions

⊥M.S.L. and T.A.W. are co-first authors. Y.T., E.F., and J.K.G. designed the experiment. S.T.R. performed the electron-beam lithography. M.S.L., T.A.W., R.V.C., A.S., and A.T.Y. carried out the X-PEEM measurements. M.S.L. and T.A.W. analyzed the data. M.S.L, T.A.W., and Y.T. cowrote the manuscript.

Notes

The authors declare no competing financial interest.

ACKNOWLEDGMENTS

Funding for these experiments was obtained from the National Science Foundation (DMR 0747896 and 1411250) and the Research Council of Norway (Contract No. 190086/S10). The Advanced Light Source is supported by the Director, Office of Science, Office of Basic Energy Sciences, of the U.S. Department of Energy (DOE) under Contract No. DE-AC02-05CH11231. Patterning of the micromagnets was carried out at the Center for Nanophase Materials Sciences, which is a U.S. DOE Office of Science User Facility.

REFERENCES

(1) Parkin, S. S. P.; Hayashi, M.; Thomas, L. Magnetic Domain-Wall Racetrack Memory. *Science* **2008**, *320*, 190−194.

(2) Parkin, S. S. P.; Yang, S.-H. Memory on the Racetrack. *Nat. Nanotechnol.* **2015**, *10*, 195−198.

(3) Hertel, R. Vortex States a La Carte. *Nat. Nanotechnol.* **2013**, *8*, 318−320.

(4) Van Waeyenberge, B.; Puzic, A.; Stoll, H.; Chou, K. W.; Tyliszczak, T.; Hertel, R.; Fahnle, M.; Bruckl, H.; Rott, K.; Reiss, G.; Neudecker, I.; Weiss, D.; Back, C. H.; Schutz, G. Magnetic Vortex Core Reversal by Excitation with Short Bursts of an Alternating Field. *Nature* **2006**, *444*, 461−464.

(5) Fert, A.; Cros, V.; Sampaio, J. Skyrmions on the Track. *Nat. Nanotechnol.* **2013**, *8*, 152−156.

(6) Nagaosa, N.; Tokura, Y. Topological Properties and Dynamics of Magnetic Skyrmions. *Nat. Nanotechnol.* **2013**, *8*, 899−911.

(7) Braun, H.-B. Topological Effects in Nanomagnetism: From Superparamagnetism to Chiral Quantum Solitons. *Adv. Phys.* **2012**, *61*, 1−116.

(8) Neubauer, A.; Pfleiderer, C.; Binz, B.; Rosch, A.; Ritz, R.; Niklowitz, P. G.; Boni, P. Topological Hall Effect in the a Phase of Mnsi. *Phys. Rev. Lett.* **2009**, *102*, 186602.

(9) Li, Y.; Kanazawa, N.; Yu, X. Z.; Tsukazaki, A.; Kawasaki, M.; Ichikawa, M.; Jin, X. F.; Kagawa, F.; Tokura, Y. Robust Formation of Skyrmions and Topological Hall Effect Anomaly in Epitaxial Thin Films of MnSi. *Phys. Rev. Lett.* **2013**, *110*, 117202.

(10) Huang, S. X.; Chien, C. L. Extended Skyrmion Phase in Epitaxial FeGe(111) Thin Films. *Phys. Rev. Lett.* **2012**, *108*, 267201.

(11) Okamura, Y.; Kagawa, F.; Mochizuki, M.; Kubota, M.; Seki, S.; Ishiwata, S.; Kawasaki, M.; Onose, Y.; Tokura, Y. Microwave Magnetoelectric Effect Via Skyrmion Resonance Modes in a Helimagnetic Multiferroic. *Nat. Commun.* **2013**, *4*, 2391.

(12) Jonietz, F.; Muhlbauer, S.; Pfleiderer, C.; Neubauer, A.; Munzer, W.; Bauer, A.; Adams, T.; Georgii, R.; Boni, P.; Duine, R. A.; Everschor, K.; Garst, M.; Rosch, A. Spin Transfer Torques in MnSi at Ultralow Current Densities. *Science* **2010**, *330*, 1648−1651.

(13) Yu, X. Z.; Kanazawa, N.; Zhang, W. Z.; Nagai, T.; Hara, T.; Kimoto, K.; Matsui, Y.; Onose, Y.; Tokura, Y. Skyrmion Flow Near Room Temperature in an Ultralow Current Density. *Nat. Commun.* **2012**, *3*, 988.

(14) Jiang, W.; Upadhyaya, P.; Zhang, W.; Yu, G.; Jungfleisch, M. B.; Fradin, F. Y.; Pearson, J. E.; Tserkovnyak, Y.; Wang, K. L.; Heinonen, O.; te Velthuis, S. G. E.; Hoffmann, A. Blowing Magnetic Skyrmion Bubbles. *Science* **2015**, *349*, 283−286.

(15) Li, J.; Tan, A.; Moon, K. W.; Doran, A.; Marcus, M. A.; Young, A. T.; Arenholz, E.; Ma, S.; Yang, R. F.; Hwang, C.; Qiu, Z. Q. Tailoring the Topology of an Artificial Magnetic Skyrmion. *Nat. Commun.* **2014**, *5*, 4704.

(16) Locquet, J. P.; Perret, J.; Fompeyrine, J.; Machler, E.; Seo, J. W.; Van Tendeloo, G. Doubling the Critical Temperature of $La_{1.9}Sr_{0.1}CuO_4$ Using Epitaxial Strain. *Nature* **1998**, *394*, 453−456.

(17) Imai, Y.; Kimura, S.; Kosemura, D.; Ogura, A. High-Resolution X-Ray Microdiffraction from a Locally Strained SOI with Width of 150 nm. *J. Phys.: Conf. Ser.* **2014**, *502*, 012026.

(18) Ulvestad, A.; Cho, H. M.; Harder, R.; Kim, J. W.; Dietze, S. H.; Fohtung, E.; Meng, Y. S.; Shpyrko, O. G. Nanoscale Strain Mapping in Battery Nanostructures. *Appl. Phys. Lett.* **2014**, *104*, 073108.

(19) Choe, S.-B.; Acremann, Y.; Scholl, A.; Bauer, A.; Doran, A.; Stohr, J.; Padmore, H. A. Vortex Core-Driven Magnetization Dynamics. *Science* **2004**, *304*, 420−422.

(20) Ramirez, A. P. Colossal Magnetoresistance. *J. Phys.: Condens. Matter* **1997**, *9*, 8171−8199.

(21) Tokura, Y. Critical Features of Colossal Magnetoresistive Manganites. *Rep. Prog. Phys.* **2006**, *69*, 797−851.

(22) Takamura, Y.; Chopdekar, R. V.; Scholl, A.; Doran, A.; Liddle, J. A.; Harteneck, B.; Suzuki, Y. Tuning Magnetic Domain Structure in Nanoscale $La_{0.7}Sr_{0.3}MnO_3$ Islands. *Nano Lett.* **2006**, *6*, 1287−1291.

(23) Folven, E.; Takamura, Y.; Grepstad, J. K. X-Peem Study of Antiferromagnetic Domain Patterns in $LaFeO_3$ Thin Films and Embedded Nanostructures. *J. Electron Spectrosc. Relat. Phenom.* **2012**, *185*, 381−388.

(24) Berndt, L. M.; Balbarin, V.; Suzuki, Y. Magnetic Anisotropy and Strain States of (001) and (110) Colossal Magnetoresistance Thin Films. *Appl. Phys. Lett.* **2000**, *77*, 2903−2905.

(25) Martin, J. I.; Nogues, J.; Liu, K.; Vicent, J. L.; Schuller, I. K. Ordered Magnetic Nanostructures: Fabrication and Properties. *J. Magn. Magn. Mater.* **2003**, *256*, 449−501.

(26) Heyderman, L. J.; Czekaj, S.; Nolting, F.; Muller, E.; Fischer, P.; Gasser, P.; Lopez-Diaz, L. Photoemission Electron Microscopy Study of Remanent Magnetic Domain States in Ferromagnetic Wedge Films Deposited on Substrates with Micrometer-Sized Square Plateaus. *J. Appl. Phys.* **2006**, *99*, 063904.

(27) Shinjo, T.; Okuno, T.; Hassdorf, R.; Shogeto, K.; Ono, T. Magnetic Vortex Core Observation in Circular Dots of Permalloy. *Science* **2000**, *289*, 930−932.

(28) Anders, S.; Padmore, H. A.; Duarte, R. M.; Renner, T.; Stammler, T.; Scholl, A.; Scheinfein, M. R.; Stohr, J.; Seve, L.; Sinkovic, B. Photoemission Electron Microscope for the Study of Magnetic Materials. *Rev. Sci. Instrum.* **1999**, *70*, 3973−3981.

(29) Vansteenkiste, A.; Leliaert, J.; Dvornik, M.; Helsen, M.; Garcia-Sanchez, F.; Van Waeyenberge, B. The Design and Verification of Mumax^3. *AIP Adv.* **2014**, *4*, 107133.

(30) Golosovsky, M.; Monod, P.; Muduli, P. K.; Budhani, R. C. Spin-Wave Resonances in $La_{0.7}Sr_{0.3}MnO_3$ Films: Measurement of Spin-Wave Stiffness and Anisotropy Field. *Phys. Rev. B: Condens. Matter Mater. Phys.* **2007**, *76*, 184413.

(31) Steenbeck, K.; Hiergeist, R. Magnetic Anisotropy of Ferromagnetic $La_{0.7}(Sr, Ca)_{0.3}MnO_3$ Epitaxial Films. *Appl. Phys. Lett.* **1999**, *75*, 1778−1780.

(32) Angeloni, M.; Balestrino, G.; Boggio, N. G.; Medaglia, P. G.; Orgiani, P.; Tebano, A. Suppression of the Metal-Insulator Transition Temperature in Thin $La_{0.7}Sr_{0.3}MnO_3$ Films. *J. Appl. Phys.* **2004**, *96*, 6387−6392.

DOI: 10.1021/acsnano.6b03770
ACS Nano 2016, 10, 8545−8551

(33) Suzuki, Y.; Hwang, H. Y.; Cheong, S.-W.; van Dover, R. B. The Role of Strain in Magnetic Anisotropy of Manganite Thin Films. *Appl. Phys. Lett.* **1997**, *71*, 140−142.
(34) Thiele, C.; Dörr, K.; Bilani, O.; Rödel, J.; Schultz, L. Influence of Strain on the Magnetization and Magnetoelectric Effect in $La_{0.7}A_{0.3}MnO_3$/PMN-PT(001) (A = Sr,Ca). *Phys. Rev. B: Condens. Matter Mater. Phys.* **2007**, *75*, 054408.
(35) Ziegler, J. F.; Ziegler, M. D.; Biersack, J. P. SRIM − the Stopping and Range of Ions in Matter (2010). *Nucl. Instrum. Methods Phys. Res., Sect. B* **2010**, *268*, 1818−1823.
(36) Rogan, R. C.; Tamura, N.; Swift, G. A.; Ustundag, E. Direct Measurement of Triaxial Strain Fields around Ferroelectric Domains Using X-Ray Microdiffraction. *Nat. Mater.* **2003**, *2*, 379−381.
(37) Folven, E.; Scholl, A.; Young, A. T.; Retterer, S.; Boschker, J. E.; Tybell, T.; Takamura, Y.; Grepstad, J. K. Effects of Nanostructuring and Substrate Symmetry on Antiferromagnetic Domain Structure in $LaFeO_3$ Thin Films. *Phys. Rev. B: Condens. Matter Mater. Phys.* **2011**, *84*, 220410.
(38) Folven, E.; Scholl, A.; Young, A. T.; Retterer, S. T.; Boschker, J. E.; Tybell, T.; Takamura, Y.; Grepstad, J. K. Crossover from Spin-Flop Coupling to Collinear Spin Alignment in Antiferromagnetic/Ferromagnetic Nanostructures. *Nano Lett.* **2012**, *12*, 2386−2390.
(39) Folven, E.; Tybell, T.; Scholl, A.; Young, A.; Retterer, S. T.; Takamura, Y.; Grepstad, J. K. Antiferromagnetic Domain Reconfiguration in Embedded $LaFeO_3$ Thin Film Nanostructures. *Nano Lett.* **2010**, *10*, 4578−4583.

DOI: 10.1021/acsnano.6b03770
ACS Nano 2016, 10, 8545−8551